8.5 Atoms in a High Laser Field

Modern developments in ultrafast laser science open new dimensions of light matter interaction and are the basis for an active, cutting edge field of research (a glimpse of the kind of processes studied today may be obtained e.g. from HICKSTEIN et al. 2012). The radiation intensity $I = W/(A\Delta t)$ in a focussed laser pulse scales with the total energy W of the pulse, its focal area A, and pulse duration Δt. Thus, the intensity of a 10 fs laser pulse is e.g. 10^6 times higher than that of a 10 ns pulse which contains the same energy W. As discussed in Sect. 8.2.2 and exemplified in Table 8.4, gigantic electric field strengths can be generated in this manner, presently surpassing the field that an electron experiences on the first BOHR orbit in the H atom by two orders of magnitude. And the experimental limits are being pushed further.

Atoms and molecules exposed to such extreme conditions, react with a wealth of astonishing new phenomena – warranting also theoretical approaches quite different from that outlined in Sect. 8.2.

8.5.1 Ponderomotive Potential

As discussed previously, an electromagnetic field interacting with a free electron cannot just transfer photon energy directly onto the electron (COMPTON scattering, as discussed in Sect. 8.4.5, is only relevant at very high photon energies $\hbar\omega$). If, however, a third body (e.g. an atomic core) is present, energy and momentum conservation may in principle be achieved with the help of this third particle. Our discussion thus starts with a very conventional approach: we solve the classical, non-relativistic equation of motion of an electron oscillating in an electric field of amplitude E_0 and frequency ω,

$$m_e \frac{dv}{dt} = eE_0 \cos \omega t,$$

and obtain velocity and kinetic energy of the electron in the stationary case:

$$v(t) = \frac{eE_0}{m_e \omega} \sin \omega t \quad \Rightarrow \quad \frac{1}{2} m_e v^2 = \frac{e^2 E_0^2}{2m_e \omega^2} \sin^2 \omega t. \tag{8.135}$$

The deflection of the electron from its average position is given by

$$x = -\frac{eE_0}{\omega^2 m_e} \cos(\omega t) = -x_0 \cos(\omega t). \tag{8.136}$$

For the oscillation amplitude one calculates with (4.2)

$$x_0 = \frac{eE_0}{\omega^2 m_e} = \frac{e}{\omega^2 m_e} \sqrt{\frac{2I}{\varepsilon_0 c}} = \frac{e\lambda^2}{4\pi^2 c^2 m_e} \sqrt{\frac{2I}{\varepsilon_0 c}}, \tag{8.137}$$

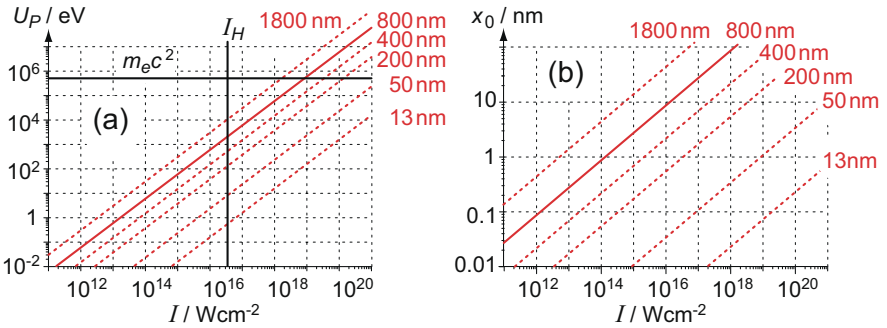

Fig. 8.28 Ponderomotive potential **(a)** and maximum amplitude of an electron **(b)** in the field of a short laser pulse of intensity I and wavelength λ; the *full red line* corresponds to the wavelength $\lambda = 800\,\text{nm}$ of the Ti:Sapph laser

which in convenient units reads:

$$x_0/\,\text{nm} = 1.3607 \times 10^{-7}[\lambda/\,\text{nm}]^2\sqrt{I/\left(10^{12}\,\text{W cm}^{-2}\right)}. \tag{8.138}$$

The average energy U_p inherent to this *quiver motion* is called *ponderomotive potential*:

$$U_\text{p} = \overline{\frac{1}{2}m_\text{e}v^2} = \frac{e^2E_0^2}{4m_\text{e}\omega^2} = \frac{1}{4}m_\text{e}\omega^2x_0^2.$$

Inserting (4.2) one obtains

$$U_\text{p} = \frac{e^2I}{2\varepsilon_0 c m_\text{e}\omega^2} = \frac{e^2I\lambda^2}{8\pi^2\varepsilon_0 c^3 m_\text{e}} \propto I\lambda^2, \quad \text{or} \tag{8.139}$$

$$U_\text{p}/\,\text{eV} = 9.3375 \times 10^{-8}[\lambda/\,\text{nm}]^2\left[I/\left(10^{12}\,\text{W cm}^{-2}\right)\right]. \tag{8.140}$$

We point out that this *expression is completely identical to* (H.20), *formally derived from the term quadratic in the vector potential* $\boldsymbol{A}$ in the exact (semiclassical) Hamiltonian (H.1) for an atom in an electromagnetic field.

The order of magnitude of U_p and x_0 is illustrated by Fig. 8.28 for a number of wavelengths λ as a function of laser intensity I. The full red lines refer to the fundamental of the Titanium-sapphire laser (short Ti:Sapph) at $\lambda = 800\,\text{nm}$ – the "work horse" of ultrafast laser science. As an example, an electron in the focus of a laser beam at an intensity of $10^{14}\,\text{W cm}^{-2}$ experiences a ponderomotive potential of $U_\text{p} = 5.976\,\text{eV}$, and according to (8.138) the corresponding excitation amplitude is $x_0 = 0.87\,\text{nm}$ – a huge electron motion as compared to typical atomic radii of 0.1 nm to 0.25 nm (see Sect. 3.1.5).

Clearly, electrons bound to an atom or molecule exposed to such field strengths will experience dramatic changes of their wave functions and term energies. We thus have to compare the ponderomotive potential (8.139) to the binding energies of the electrons in atoms. In the low intensity limit, we expect energy shifts as we have

derived them for the dynamic STARK effect in (8.97). And indeed, a comparison with (8.139) shows that in the limit of high frequencies $\omega \gg \omega_{ba}$, with $\sum \mathrm{f}_{ba}^{(\mathrm{opt})} = 1$ both expressions become identical.

However, for really intense laser fields, in particular at longer wavelengths as characterized in Fig. 8.28, a complete break down of the bound state description developed so far in atomic physics is expected. Two specific limits are indicated: on the one hand, the system becomes highly relativistic if $U_\mathrm{p} > m_\mathrm{e}c^2$. The intensity necessary to reach this limit decreases according to (8.139) with the square of the wavelength. On the other hand, for intensities above I_H the electric field in the laser focus is larger than the atomic field E_H that an electron experiences in the H atom at a distance a_0 from the nucleus. This intensity is independent of wavelength:

$$I_H = \frac{\varepsilon_0 c}{2} E_H^2 = \frac{\varepsilon_0 c}{2} \left(\frac{e}{4\pi\,\varepsilon_0 a_0^2} \right)^2 = 3.51 \times 10^{16}\,\mathrm{W\,cm^{-2}}\,. \tag{8.141}$$

8.5.2 KELDISH Parameter

There are other aspects for considering a laser field to be high. One of these is derived from the ratio of ionization potential W_I to ponderomotive potential U_p. For reasons to be discussed in Sect. 8.5.4 one defines the so called

$$\text{KELDYSH } \textit{parameter} \quad \gamma = \sqrt{\frac{W_I}{2U_\mathrm{p}}} = \sqrt{\frac{\varepsilon_0 c m_\mathrm{e} \omega^2 W_I}{e^2 I}} \tag{8.142}$$

$$\text{or} \quad \text{in numerical terms} \qquad \gamma = 2.31 \times 10^3 \sqrt{\frac{W_I/\mathrm{eV}}{I/10^{12}\,\mathrm{W\,cm^{-2}}\,\lambda/\mathrm{nm}^2}}$$

introduced in the pioneering work of KELDYSH (1965). This parameter characterizes the transition from *atom with laser field* $\gamma > 1$ to a situation that one may describe as *laser field with atom* $\gamma < 1$. For the above example, an H atom with $W_I = 13.6\,\mathrm{eV}$ in a radiation field with $I = 10^{14}\,\mathrm{W\,cm^{-2}}$ at $\lambda = 800\,\mathrm{nm}$ we find $\gamma \sim 1$. At this intensity the atomic energy is thus comparable with the energy imposed onto the electron by the laser field. For an H atom, this may be called an intense laser field. We also emphasize at this point that the KELDYSH parameter depends on the wavelength: the longer the wavelength, the more efficient is the laser field!

8.5.3 From Multi-photon Ionization to Saturation

Multi-photon ionization (MPI) has already been subject to our discussion in Sect. 5.5.5. There we have used perturbation theory: up to $\mathcal{N}$th order for $\mathcal{N}$ photon absorption. As described there, the cross section for MPI depends on the laser

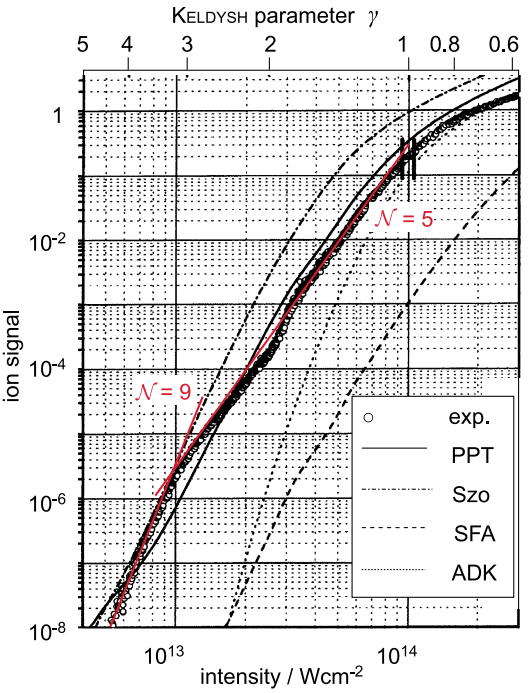

Fig. 8.29 Multi-photon ionization signal from Xe at 800 nm as a function of laser intensity according to LAROCHELLE et al. (1998). The slope in the *log–log* display gives with (5.92) an indication of the number of photons $\mathcal{N}$ involved in the process. Sketched in *red* are the slopes for processes with $9\hbar\omega$ and $5\hbar\omega$, respectively. For the direct MPI of Xe at least 9 photons are needed – observed for the lowest intensities. At an intensity $I = 10^{14}\,\mathrm{W\,cm^{-2}}$ the process is saturated. The ion yield is compared with different theories

intensity as $\propto I^{\mathcal{N}}$. However, if the laser field becomes comparable to inner-atomic fields this approach is bound to break down. Atoms and molecules often behave quite surprisingly in high laser fields: one even finds that the processes become more and more classical as intensities increase. For instance, at very high intensities atomic energy levels are shifted substantially and electrons can escape from the atoms by tunnelling or "above-barrier" processes, as we shall see in a moment. Their kinetic energies then increase as laser intensity increases – a phenomenon in direct contrast to the canonical observations with the photoelectric effect at low intensities.

The transition between perturbative, tunnelling, and above-barrier region is, however, seamless. A "benchmark" type of experiment is shown in Fig. 8.29. It has been reported by LAROCHELLE et al. (1998), who very carefully measured the MPI yield from Xe with femtosecond laser pulses at 800 nm. The ionization potential of Xe is $W_I = 13.44\,\mathrm{eV}$, and with $W_I/\hbar\omega = 8.67$ the number of photons required for ionization is 9. With an ion yield $\propto I^{\mathcal{N}}$ one would, in a double logarithmic plot, expect a slope of $\mathcal{N} = 9$. As illustrated in Fig. 8.29 this is indeed the case for the lowest intensities, while at intermediate intensities the experimental data appear to follow a power law I^5, as indicated in the graph. Xe is a quite complex atom with dense series of states above the first excited state, the latter requiring ca. 5 photons to be excited. Obviously at such high intensities the resonance condition is washed out due to the dynamic STARK effect, and after this first step has been reached the subsequent ionization of this state occurs readily.

As also seen in Fig. 8.29 the rise of the ion yield above ca. $10^{14}\,\mathrm{W\,cm^{-2}}$ continues to decrease dramatically. One may conclude that at these intensities almost all atoms are already ionized in the centre of the laser focus – one speaks of saturation. The continuing rise with intensity is essentially due to a geometrical effect: enhanced ionization now also occurs of the peripheral zone of the laser beam (having a Gaussian profile). Thus, the volume in which saturation intensity is reached increases, and with it the total ion yield. The upper scale in Fig. 8.29 gives the KELDYSH parameter (8.142) for comparison. Saturation intensity obviously corresponds to $\gamma \simeq 1$, that is to say saturation sets in where the moderate field becomes a very high one.

8.5.4 Tunnelling Ionization

At very high intensities the internal atomic field will be modified substantially by the external (oscillating) electric field. Lets assume the atomic potential to be Coulombic with charge Ze. When adding a linearly polarized laser field, an atomic electron 'sees' a time dependent, overall potential

$$V(r,t) = -\frac{Ze^2}{4\pi\varepsilon_0 r} - eE(t)z \quad \text{with } z = r\cos\theta, \tag{8.143}$$

as illustrated in Fig. 8.30 for the time of maximum field (amplitude E_0).

A bound electron can thus "tunnel out" of the atom as indicated in Fig. 8.30**(a)** or may even leave the atom "above-barrier" **(b)**, if the latter is lowered sufficiently. This happens at a critical intensity I_{cr} when at the saddle point $V(r_{\mathrm{s}}) = -W_I$. From $\mathrm{d}V(r)/\mathrm{d}r|_{r_{\mathrm{s}}} = 0$ one finds

$$I_{\mathrm{cr}} = \frac{\pi^2 c\varepsilon_0^3}{2Z^2e^6}(W_I)^4 \tag{8.144}$$

$$\frac{I_{\mathrm{cr}}}{\mathrm{W\,cm^{-2}}} \simeq \frac{4.0\times10^9}{Z^2}\left(\frac{W_I}{\mathrm{eV}}\right)^4.$$

For an H atom ($Z = 1$, $W_I = E_{\mathrm{h}}/2$), the critical intensity is $I_c = 1.37 \times 10^{14}\,\mathrm{W\,cm^{-2}}$ – which is easily reached in a focused femtosecond laser pulse.

In this picture the KELDYSH parameter may be visualized in an alternative interpretation: since the laser field oscillates, the crucial question is, whether the electron can escape the atom fast enough before the field reverses its sign. Considering Fig. 8.30**(a)**, one estimates the distance ℓ_{tu} through which the electron has to tunnel – for simplicity from a so called "zero range potential" (red dashed line). From Fig. 8.30**(a)** one reads:

$$\ell_{\mathrm{tu}} = W_I/(eE_0) \tag{8.145}$$

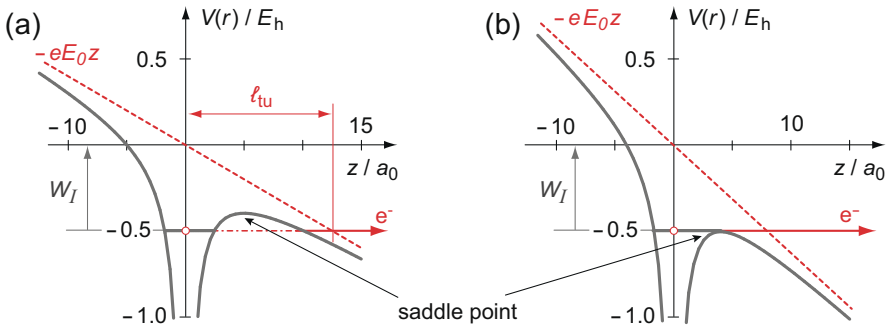

Fig. 8.30 Model to understand atomic ionization in a high electric field, in particular in an intense laser field: **(a)** tunnelling **(b)** electron emission "above-barrier". Sketched are cuts through the potential parallel to the direction of the $\boldsymbol{E}$ field at the time of maximum field in z-direction

As the electron leaves the atom its kinetic energy is $W_{\text{kin}} = W_I$, its velocity $v = \sqrt{2W_I/m_\text{e}}$, and consequently the tunnelling time becomes[6]

$$t_{\text{tu}} = \frac{\ell_{\text{tu}}}{v} = \frac{\sqrt{m_\text{e} W_I}}{\sqrt{2}eE_0} = \frac{\sqrt{\varepsilon_0 c m_\text{e} W_I}}{2\sqrt{e^2 I}}. \tag{8.146}$$

In order to allow the electrons to leave that atom for good, the tunnelling time must be distinctively smaller than one half of the oscillation period, say $t_{\text{tu}} < 1/(2\omega)$. One then defines the KELDYSH parameter as

$$\gamma = 2\omega t_{\text{tu}} = \sqrt{\frac{\varepsilon_0 c m_\text{e} \omega^2 W_I}{e^2 I}}, \tag{8.147}$$

in agreement with (8.142). Saturation of the ion signal, observed in Fig. 8.29 for high laser intensities ($\gamma \lesssim 1$), is thus found to happen at intensities and frequencies for which the electron has sufficient time to escape when the oscillation field reaches its maximum value E_0. With this visualization of the ionization process it is obvious that ionization is more probable when the field oscillates less frequently, i.e. at larger wavelengths.

The essentially classical ADK theory (AMMOSOV et al. 1986), often used with astonishingly good results for atoms, neglects the frequency dependence of the process completely. It considers saturation to be reached when the field is high enough for direct "above-barrier" ionization as sketched in Fig. 8.30**(b)**. To give a typical value: in the H atom at $\lambda = 800\,\text{nm}$, $\gamma = 0.9$ when this critical field intensity (8.144) is reached. A detailed understanding of the relevant processes is subject to current research. Some important concepts and consequences will be discussed in the following.

[6] One should take this with a grain of salt: Tunnelling is a quantum mechanical process, while in a classical picture the electron can only leave the atom "above-barrier".

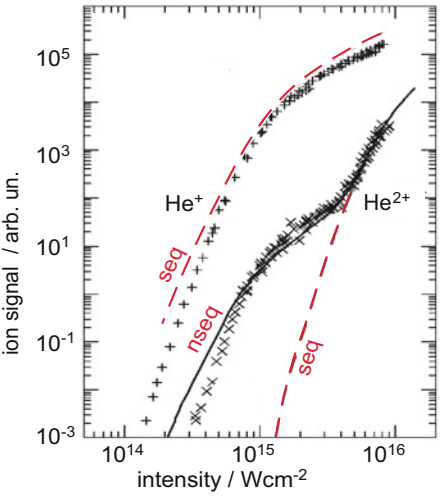

Fig. 8.31 Non-sequential double ionization of He by multi-photon processes with 160 fs pulses at 780 nm and comparison with different theories according to WATSON et al. (1997). The He^+ (+) and He^{2+} (×) ion yield has been measured by WALKER et al. (1994). The *dashed red lines* (seq) represent a theory with one active electron only, the *full black line* (nseq) is a model calculation for non-sequential ionization

8.5.5 Recollision

If the timing between laser field and electron ejection is favourable, the electron may even return to the atom. This so called *rescattering of electrons* was first discussed in a pioneering paper by CORKUM (1993). In a high, oscillating electric field the trajectory of an electron depends of course on the exact point in time when it starts. A simple classical calculation shows that the electron returns indeed to its starting point, if is has not yet travelled too far when the sign of the electric field is reversed. CORKUM found, that (at the origin) the *rescattered electron can acquire a kinetic energy* of up to

$$3.17 \times U_\mathrm{p} \geq W_\mathrm{kin}^{(\mathrm{el})}. \tag{8.148}$$

This happens for an electron ejected at time $t = 0$, if the phase angle of the field $E(t) \propto \cos(\omega t + \phi)$ is $\phi \simeq 17°$. The physics of these backscattered electrons is very interesting and continues to be a hot topic in current research.

One phenomenon associated with back scattered electrons is the ejection of a second electron, leading to the so called *non-sequential double ionization.* It can be recognized by a very special behaviour of the MPI cross section as a function of laser intensity, illustrated for He as an example in Fig. 8.31.

Generally speaking, one expects processes of the following type for a multi-electron system A:

$$\begin{aligned}
\mathrm{A} + \mathcal{N}_1 \hbar\omega &\rightarrow \mathrm{A}^+ + \mathrm{e}^- \\
\mathrm{A}^+ + \mathcal{N}_2 \hbar\omega &\rightarrow \mathrm{A}^{2+} + \mathrm{e}^- \\
&\cdots \\
\mathrm{A}^{q+} + \mathcal{N}_{q+1} \hbar\omega &\rightarrow \mathrm{A}^{(q+1)+} + \mathrm{e}^-.
\end{aligned}$$

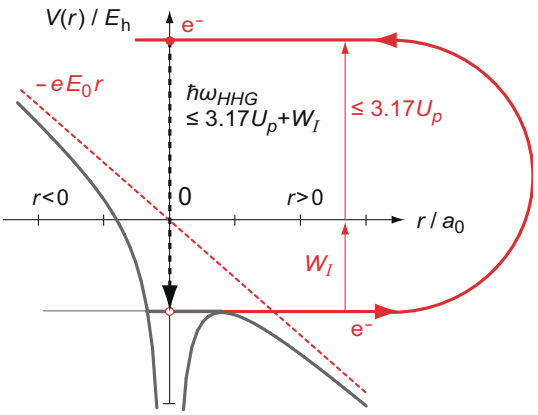

Fig. 8.32 Visualization for the generation of high harmonics (HHG). If the electron is emitted "above-barrier" at the right time it may be *back scattered* by the inverting field with a kinetic energy up to $W_{\mathrm{kin}} \leq 3.17U_{\mathrm{p}}$. This energy + ionization potential is then available in principle for HHG

If these processes occur consecutively one speaks of stepwise or sequential ionization. But in the case of strongly correlated systems one may also consider non-sequential ionization, i.e. the simultaneous emission of several electrons in one genuine multi-electron process. Alternatively, two electrons may be ejected by a recolliding electron as discussed – in summary

$$\mathrm{A} + N_1\hbar\omega \rightarrow \mathrm{A}^+ + \mathrm{e}^- \left(W_{\mathrm{kin}}^{(\mathrm{el})} \leq 3.17U_{\mathrm{p}}\right)$$
$$\mathrm{A}^{2+} + 2\mathrm{e}^- \leftarrow \mathrm{A}^+ + \mathrm{e}^- \hookleftarrow,$$

which is also a non-sequential ionization process. Characteristic for non-sequential ionization is the kink in the double logarithmic plot of the ion yield as a function of intensity – very clearly seen for He^{++} in Fig. 8.31.

8.5.6 High Harmonic Generation (HHG)

Rescattered electrons cannot only eject a second electron. They may also be recaptured by the ion and emit electromagnetic radiation during this process: this leads to the generation of electromagnetic waves with frequencies that are multiples of the original laser frequency (fundamental). This process is called *high harmonic generation* (HHG) and has attracted worldwide considerable interest during the past years.

The HHG mechanism is illustrated schematically in Fig. 8.32. The recolliding electron has a potentially high excess energy that may be emitted during the capture process as radiation. According to (8.148), the energy of the recolliding electron can be as high as $3.17U_{\mathrm{p}}$. Thus, photon energies up to $\hbar\omega_{\mathrm{HHG}} \leq 3.17U_{\mathrm{p}} + W_I$ may be emitted upon capture of the electron.

This HHG process is used in current research very successfully to generate short pulses in the soft X-ray region (XUV). An intense femtosecond laser pulse is focussed into a dense gas target (e.g. a gas jet, a gas filled cell or capillary). One

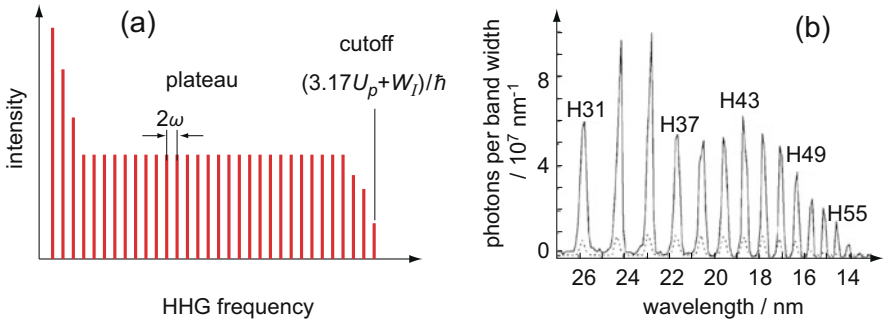

Fig. 8.33 **(a)** Schematic HHG spectrum with plateau and cutoff at $3.17U_\mathrm{p} + W_I$. The frequency distances are 2ω. **(b)** Example of an experimentally observed HHG spectrum from BALCOU et al. (2002). 30 fs pulses at ca. 800 nm were focussed into a Ne gas jet. Different focussing conditions (*full and dotted lines*) lead to quite different efficiencies

obtains the XUV radiation in forward direction. Typically it contains a broad spectrum of harmonics $\omega_\mathrm{HHG} = (2\mathcal{N} + 1)\omega$ of the fundamental ω as shown schematically in Fig. 8.33**(a)**. For symmetry reasons, usually only odd harmonics are emitted.

The scheme indicates the particularly high efficiency for low harmonics, followed by a long "plateau" with frequencies at a distance of 2ω up to the so called *cutoff* at $3.17U_\mathrm{p} + W_I$, which is easily understood in view of Fig. 8.32. In Fig. 8.33**(b)** gives as a typical experimental example the spectrum of Ne. As shown in the figure one may modify the emitted output by judicious choice of focussing conditions. This is a consequence of the highly nonlinear process. Optimization of HHG generation for practical application is currently a hot topic in AMO research. Special temporal and spatial pulse shaping may be used to improve the conversion efficiency substantially. HHG is currently being used as a convenient, table top, time resolved short pulse radiation source in the near X-ray region. It has considerable application potential for X-ray spectroscopy. The shortest wavelengths achievable depend on the target, on the pump laser intensity, as well as on its frequency (since $U_\mathrm{P} \propto \lambda^2$).

During the past decade the generation of *attosecond laser pulses* ($1\,\mathrm{as} = 10^{-18}\,\mathrm{s}$) by superposition of several harmonics has developed very successfully (see e.g. the reviews by KRAUSZ and IVANOV 2009; SANSONE et al. 2011). As it turns out, the harmonics generated are coherent; superposing them artfully (see e.g. TZALLAS et al. 2003) and filtering the resulting radiation suitably corresponds to interference in a FOURIER series, leading to a sequence of pulses with an individual pulse duration below 1 fs. As always, a new method that improves earlier techniques by one or two orders of magnitude opens new perspectives with an unforeseeable potential in basic research and applications. Certainly we shall witness exciting developments of "*attosecond science*" in the years to come (as illustrated e.g. by SANSONE et al. 2010; BOGUSLAVSKIY et al. 2012; VRAKKING and ELSAESSER 2012).

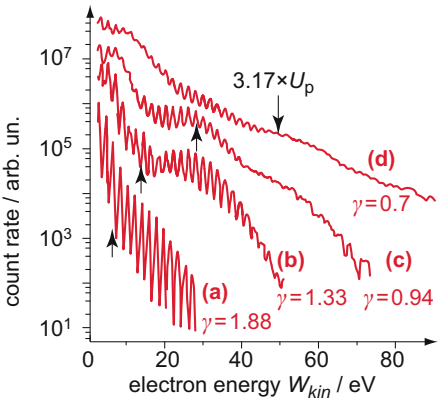

Fig. 8.34 ATI spectra of Ar according to PAULUS et al. (1994), obtained with 40 fs, 630 nm laser pulses at intensities of **(a)** $6 \times 10^{13}\,\mathrm{W\,cm^{-2}}$, **(b)** $1.2 \times 10^{14}\,\mathrm{W\,cm^{-2}}$, **(c)** $2.4 \times 10^{14}\,\mathrm{W\,cm^{-2}}$ and **(d)** $4.4 \times 10^{14}\,\mathrm{W\,cm^{-2}}$ (the traces are vertically slightly displaced for better visibility); the *black arrows* indicate the maximum classical back scattering energy of $3.17 \times U_p$

8.5.7 Above-Threshold Ionization in High Laser Fields

Before ending this chapter we return briefly to ATI processes which we have introduced already in Sect. 5.5.5. The question here is, how these processes change as the laser intensity is increasing – from MPI through the tunnelling regime and to above-barrier ionization?

As a particularly suggestive example we show in Fig. 8.34 the spectra for Ar that were studied by PAULUS et al. (1994) with beautifully resolved ATI peaks. Argon has an ionization potential of $\simeq$15.4 eV, according to (8.147) the laser intensities used here thus correspond to KELDYSH parameters γ of **(a)** 1.88, **(b)** 1.33, **(c)** 0.94 and **(d)** 0.7 – a range covering the critical transition from moderate to above-barrier behaviour. This is reflected quite evidently in the electron spectra: while at the lowest intensity **(a)** an unspectacular ATI spectrum is observed, quite comparable to that shown in Fig. 5.13 for Xe, the higher intensities promote very pronounced structures as a function of electron energy, that remind us of the plateau seen in HHG which we have discussed in the last section. There, the cutoff was identified as corresponding to the maximum energy of rescattered electrons.

Thus it appears self-evident to attribute the plateaus or beats in the ATI spectra also to recollision: obviously recolliding electrons too may absorb further photons. Without going into the finer details of these observations we indicate by arrows in Fig. 8.34 the maximum kinetic energy $3.17 \times U_p$ of the rescattered electrons. Obviously, there is even more structure and one should not over-stress the simple rescattering model for such a highly complex process. We just mention that serious quantum mechanical model calculations achieve very good agreement with the experimental data.

It is interesting to note that ATI may also be observed when ionizing quite large molecules by (moderately) high intensity lasers. This is exemplified in Fig. 8.35 for C_{60} according to CAMPBELL et al. (2000). The ionization potential is in this case ca. 7.6 eV, much lower than for argon. The intensities are thus equivalent to those used in Fig. 8.34 as documented by the corresponding KELDYSH parameters γ. Here too one may recognize, albeit weakly, something like a prolonged plateau for the higher

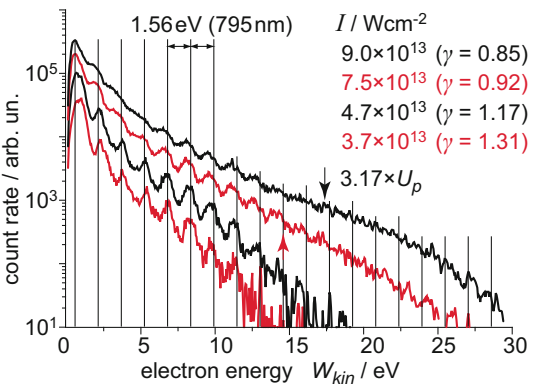

Fig. 8.35 ATI spectra of C_{60} according to CAMPBELL et al. (2000); the laser intensities for the four traces is given in the legend. The *vertical, grey lines* spaced at a distance of the photon energy (for 795 nm) allow identification of the ATI peaks

intensities. Clearly the decrease of the electron signal beyond the $3.17 \times U_p$ limit is significantly slower for higher intensities. It is also evident that in this case the laser intensity must not get too high as the clear ATI peaks in the electron spectrum smear out: this large, finite system has many active electrons (there are 240 valence electrons in C_{60}). Interaction among them thermalizes the electron motion at the highest laser intensities. Similar trends may be recognized for Ar: in that sense, C_{60} with its high symmetry may be seen as a kind of "super atom".

Section summary

- Today's short pulse lasers allow one to generate extremely high intensities I of electromagnetic radiation. The corresponding electric field strengths can easily surpass the inner atomic electric fields, even by orders of magnitude. Correspondingly, in the Hamiltonian the term quadratic to the vector potential of the field must be considered. It gives rise to the ponderomotive potential (8.140), $U_p \propto I\lambda^2$.
- The KELDYSH parameter $\gamma = \sqrt{W_I/2U_p}$ characterizes the field strengths: it is considered to be high for $\gamma \lesssim 1$.
- "Recollision" of the electron – ejected by the field and forced to return to the atom by the field – provides a useful concept for understanding non-sequential ionization, HHG and ATI in high intensity fields. A recolliding electron may acquire a kinetic energy up to $3.17 \times U_p$.
- HHG by intense femtosecond laser pulses offers excellent perspectives for time resolved spectroscopy with short X-ray pulses. It is also the basis attosecond pulses.

Acronyms and Terminology

ADK: 'AMMOSOV, DELONE, and KRAINOV', (1986) theory for strong field ionization (see e.g. Sect. 8.30).

AMO: 'Atomic, molecular and optical', physics.
ATI: 'Above-threshold ionization', in multi-photon ionization, if more photons are absorbed than necessary for ionization.
a.u.: 'atomic units', see Sect. 2.6.2.
DC: 'Direct current', unidirectional electric voltage and current.
E1: 'Electric dipole', transitions induced by the interaction of an electric dipole with the electric field component of electromagnetic radiation.
EPR: 'Electron paramagnetic resonance', spectroscopy, also called *electron spin resonance* ESR (see Sect. 9.5.2).
esu: 'electrostatic units', old system of unities, equivalent to the GAUSS system for electric quantities (see Appendix A.3).
FS: 'Fine structure', splitting of atomic and molecular energy levels due to spin orbit interaction and other relativistic effects (Chap. 6).
good quantum number: 'Quantum number for eigenvalues of such observables that may be measured simultaneously with the HAMILTON operator (see Sect. 2.6.5)'.
HHG: 'High harmonic generation', in intense laser fields.
HV: 'High voltage', electric voltages typically higher than 1000 V.
IR: 'Infrared', spectral range of electromagnetic radiation. Wavelengths between 760 nm and 1 mm according to ISO 21348 (2007).
LHC: 'Left hand circularly', polarized light, also σ^+ light.
MPI: 'Multi-photon ionization', ionization of atoms or molecules by simultaneous absorption of several photons.
NIST: 'National institute of standards and technology', located at Gaithersburg (MD) and Boulder (CO), USA. http://www.nist.gov/index.html.
NMR: 'Nuclear magnetic resonance', spectroscopy, a rather universal spectroscopic method for identifying molecules (see Sect. 9.5.3).
QED: 'Quantum electrodynamics', combines quantum theory with classical electrodynamics and special relativity. It gives a complete description of light-matter interaction.
RHC: 'Right hand circularly', polarized light, also σ^- light.
SI: 'Système international d'unités', international system of units (m, kg, s, A, K, mol, cd), for details see the website of the Bureau International des Poids et Mésure http://www.bipm.org/en/si/ or NIST http://physics.nist.gov/cuu/Units/index.html.
SVE: 'Slowly varying envelope', approximation for electromagnetic waves (see Sect. 1.2.1, specifically Eq. (1.38), Vol. 2).
Ti:Sapph: 'Titanium-sapphire laser', the 'workhorse' of ultra fast laser science.
UV: 'Ultraviolet', spectral range of electromagnetic radiation. Wavelengths between 100 nm and 400 nm according to ISO 21348 (2007).
VIS: 'Visible', spectral range of electromagnetic radiation. Wavelengths between 380 nm and 760 nm according to ISO 21348 (2007).
VUV: 'Vacuum ultraviolet', spectral range of electromagnetic radiation. part of the UV spectral range. Wavelengths between 10 nm and 200 nm according to ISO 21348 (2007).

XUV: 'Soft X-ray (sometimes also extreme UV)', spectral wavelength range between 0.1 nm and 10 nm according to ISO 21348 (2007), sometimes up to 40 nm.

References

AMMOSOV, M. V., N. B. DELONE and V. P. KRAINOV: 1986. 'Tunnel ionization of complex atoms and of atomic ions in an alternating electromagnetic field'. *Sov. Phys. JETP*, **64**, 1191–1194.

BALCOU, P. et al.: 2002. 'High-order-harmonic generation: towards laser-induced phase-matching control and relativistic effects'. *Appl. Phys. B*, **74**, 509–515.

BERGER, M. J., J. H. HUBBELL, S. M. SELTZER, J. CHANG, J. S. COURSEY, R. SUKUMAR, D. S. ZUCKER and K. OLSEN: 2010. 'XCOM: Photon cross sections database (version 1.5)', NIST. http://physics.nist.gov/xcom, accessed: 8 Jan 2014.

BOGUSLAVSKIY, A. E., A. E. BOGUSLAVSKIY, J. MIKOSCH, A. GIJSBERTSEN, M. SPANNER, S. PATCHKOVSKII, N. GADOR, M. J. J. VRAKKING and A. STOLOW: 2012. 'The multielectron ionization dynamics underlying attosecond strong-field spectroscopies'. *Science*, **335**, 1336–1340.

BORN, M. and E. WOLF: 2006. *Principles of Optics*. Cambridge University Press, 7th (expanded) edn.

BOYD, R., O. HESS, C. DENZ and E. PASPALKALIS: 2010. 'Slow light'. *J. Opt.*, **12**, 100301.

BOYD, R. W. and D. J. GAUTHIER: 2002. '"Slow" and "fast" light'. In: 'Progress in Optics', vol. 43, 497–530. Amsterdam: Elsevier.

BREIT, G. and I. I. RABI: 1931. 'Measurement of nuclear spin'. *Phys. Rev.*, **38**, 2082–2083.

BUCKINGHAM, A. D.: 1967. 'Permanent and induced molecular moments and long-range intermolecular forces'. *Adv. Chem. Phys.*, **12**, 107.

CAMPBELL, E. E. B., K. HANSEN, K. HOFFMANN, G. KORN, M. TCHAPLYGUINE M. WITTMANN and I. V. HERTEL: 2000. 'From above threshold ionization to statistical electron emission: the laser pulse-duration dependence of C_{60} photoelectron spectra'. *Phys. Rev. Lett.*, **84**, 2128–2131.

CHANTLER, C. T., K. OLSEN, R. A. DRAGOSET, J. CHANG, A. R. KISHORE, S. A. KOTOCHIGOVA and D. S. ZUCKER: 2005. 'X-ray form factor, attenuation, and scattering tables (version 2.1)', NIST. http://physics.nist.gov/ffast, accessed: 7 Jan 2014.

CORKUM, P. B.: 1993. 'Plasma perspective on strong-field multi-photon ionization'. *Phys. Rev. Lett.*, **71**, 1994–1997.

HANSON, A. L.: 1986. 'The calculation of scattering cross-sections for polarized X-rays'. *Nucl. Instrum. Methods A*, **243**, 583–598.

HAU, L. V., S. E. HARRIS, Z. DUTTON and C. H. BEHROOZI: 1999. 'Light speed reduction to 17 meters per second in an ultracold atomic gas'. *Nature*, **397**, 594–598.

HICKSTEIN, D. D. et al.: 2012. 'Direct visualization of laser-driven electron multiple scattering and tunneling distance in strong-field ionization'. *Phys. Rev. Lett.*, **109**, 073004.

HUBBELL, J. H., W. J. VEIGELE, E. A. BRIGGS, R. T. BROWN, D. T. CROMER and R. J. HOWERTON: 1975. 'Atomic form factors, incoherent scattering functions, and photon scattering cross sections'. *J. Phys. Chem. Ref. Data*, **4**, 471–538.

ISO 21348: 2007. 'Space environment (natural and artificial) – process for determining solar irradiances'. *International Organization for Standardization*, Geneva, Switzerland.

KANE, P. P., L. KISSEL, R. H. PRATT and S. C. ROY: 1986. 'Elastic-scattering of gamma-rays and X-rays by atoms'. *Phys. Rep.*, **140**, 75–159.

KELDYSH, L. V.: 1965. 'Ionization in the field of a strong electromagnetic wave'. *Sov. Phys. JETP*, **20**, 1307.

KRAUSZ, F. and M. IVANOV: 2009. 'Attosecond physics'. *Rev. Mod. Phys.*, **81**, 163–234.

LAROCHELLE, S., A. TALEBPOUR and S. L. CHIN: 1998. 'Non-sequential multiple ionization of rare gas atoms in a ti:sapphire laser field'. *J. Phys. B, At. Mol. Opt. Phys.*, **31**, 1201–1214.

LORENTZ, H. A. and P. ZEEMAN: 1902. 'The NOBEL prize in physics: in recognition of the extraordinary service they rendered by their researches into the influence of magnetism upon radiation phenomena', Stockholm. http://nobelprize.org/nobel_prizes/physics/laureates/1902/.

MENENDEZ, J. M., I. MARTIN and A. M. VELASCO: 2005. 'The stark effect in atomic Rydberg states through a quantum defect approach'. *Int. J. Quant. Chem.*, **102**, 956–960.

PAULUS, G. G., W. NICKLICH, H. L. XU, P. LAMBROPOULOS and H. WALTHER: 1994. 'Plateau in above-threshold ionization spectra'. *Phys. Rev. Lett.*, **72**, 2851–2854.

POLYANSKIY, M.: 2012. 'RefractiveIndex.Info', MediaWiki. http://refractiveindex.info, accessed: 10 Jan 2014.

SANSONE, G., L. POLETTO and M. NISOLI: 2011. 'High-energy attosecond light sources'. *Nat. Photonics*, **5**, 656–664.

SANSONE, G. et al.: 2010. 'Electron localization following attosecond molecular photoionization'. *Nature*, **465**, 763–767.

STARK, J.: 1919. 'The NOBEL prize in physics: for his discovery of the Doppler effect in canal rays and the splitting of spectral lines in electric fields', Stockholm. http://nobelprize.org/nobel_prizes/physics/laureates/1919/.

SVEN GATO REDSUN: 2004. '$3j6j9j$-symbol java calculator', Sven Gato Redsun. http://www.svengato.com/, accessed: 8 Jan 2014.

TZALLAS, P., D. CHARALAMBIDIS, N. A. PAPADOGIANNIS, K. WITTE and G. D. TSAKIRIS: 2003. 'Direct observation of attosecond light bunching'. *Nature*, **426**, 267–271.

VRAKKING, M. J. J. and T. ELSAESSER: 2012. 'X-ray photonics: X-rays inspire electron movies'. *Nat. Photonics*, **6**, 645–647.

WALKER, B., B. SHEEHY, L. F. DIMAURO, P. AGOSTINI, K. J. SCHAFER and K. C. KULANDER: 1994. 'Precision-measurement of strong-field double-ionization of helium'. *Phys. Rev. Lett.*, **73**, 1227–1230.

WATSON, J. B., A. SANPERA, D. G. LAPPAS, P. L. KNIGHT and K. BURNETT: 1997. 'Nonsequential double ionization of helium'. *Phys. Rev. Lett.*, **78**, 1884–1887.

ZIMMERMAN, M. L., M. G. LITTMAN, M. M. KASH and D. KLEPPNER: 1979. 'Stark structure of the Rydberg states of alkali-metal atoms'. *Phys. Rev. A*, **20**, 2251–2275.